Simulations of the Inelastic Response of Silicon to Shock Compression

P. G. Stubley[a], A. Higginbotham[b,*], J. S. Wark[a]

[a] *Department of Physics, Clarendon Laboratory, University of Oxford, Parks Road, Oxford OX1 3PU, UK*
[b] *York Plasma Institute, Department of Physics, University of York, York, YO10 5DD, UK*

Abstract

Recent experiments employing nanosecond white-light x-ray diffraction have demonstrated a complex response of pure, single crystal silicon to shock compression on ultra-fast timescales. We present here details of a Lagrangian code which tracks both longitudinal and transverse strains, and successfully reproduces the experimental response by incorporating a model of the shock-induced, yet kinetically inhibited, phase transition. This model is also shown to reproduce results of classical molecular dynamics simulations of shock compressed silicon.

Keywords: Silicon, Shock-compression, Molecular Dynamics, Phase-change, Lagrangian elastic code.

1. Introduction

The response of matter to rapid shock compression has been a field of study for well over a century. One material that has been a subject of particular interest for several decades is single crystal silicon [1, 2, 3, 4]. Given that this element can be manufactured in an almost perfect, defect-free form, it might first appear to be an ideal test-bed for studying the fundamental physics of shock compression. However, in many ways the opposite has seemed to be true, in that despite many attempts, a full understanding of how such perfect single crystals react at the lattice level to rapid uniaxial loading has remained surprisingly elusive, with apparently differing results and interpretations being put forward between gas gun experiments [5, 6] and those performed on a shorter time-scale employing laser-plasma-based drivers [7].

However, recent work employing nanosecond white-light Laue diffraction to diagnose laser-driven shocks in single crystal silicon shocked along the [100] axis has re-confirmed that a complex elastic response, first observed by Loveridge-Smith *et al.* [7], indeed occurs [8]. This work showed that when silicon is shock-compressed to stresses in the regime of a few 10's of GPa on nanosecond timescales, a leading double elastic-wave structure can form in compression, which, upon breakout from a free surface, can also result in a state of elastic tension.

In the work of reference [8], it was shown that the observed experimental results were consistent with simulations based on a simple Lagrangian code, which incorporated in an empirical manner a pressure dependent, but kinetically inhibited (delayed) phase transition, with the complex elastic behaviour being a result of the relatively large volume collapse associated with the change in phase. However, within the work of [8], for the sake of brevity no details of the code, and the assumptions that underpin it, were presented. Within the paper presented here we rectify this situation, giving a full description of the code, and a description of how states of strain within the shocked sample are determined, allowing us to predict time-dependent x-ray diffraction patterns that can be compared directly with experimental results.

Before describing the code in detail, we briefly recap the main features of the particular experiment it is designed to model. Within this experiment, 30 μm thick samples of [001] silicon, over-coated with a 15 μm layer of parylene-N ablator, were shock compressed by irradiation with a 5 ns square pulse of 351 nm light at an irradiance of 4×10^{14} Wcm^{-2}. At a time of 5 ns after the onset of this drive pulse, a laser-plasma-generated, quasi-white-light beam of x-rays (3-10 keV) were diffracted from the rear undriven surface of the target, with the x-rays being collimated such that they impinged on a central region of 0.8 mm diameter directly opposite the 5 mm diameter drive spot. The timing of the x-rays was such that they were diffracted from as-yet unshocked material, as well as the elastic compression waves that moved toward the rear surface of the target, and also the regions of tension that formed upon shock breakout. Further and more complete details of the experimental set-up can be found in reference [8].

In order to model the sample response we utilise and adapt a simple two-step algorithm to solve the elasticity equations within a Lagrangian framework put forward by Horie [9]. As we show below, this model allows us to keep track of the time and space-dependent elastic strains within the sample, and subsequently from them predict x-ray diffraction patterns. This approach has recently proven to be successful in modelling femtosecond diffrac-

*Corresponding author
Email address: andrew.higginbotham@york.ac.uk (A. Higginbotham)

tion patterns recorded from copper as it is shock compressed on picosecond timescales [10, 11].

The paper is laid out in the following manner. Firstly the relevant phase transition in silicon is introduced, followed by the formalism for the elastic code, including the equations that govern the phase transition. We discuss the necessary prerequisites for the code's function, and the extent of fitting required. Finally, we show a comparison between the new code and molecular dynamics simulations, before making concluding remarks.

2. Theory

2.1. Cubic diamond → β-Sn transition in silicon

We start by summarising the physics of the relevant phase transition in silicon; the first order transition from the ambient phase, which has a cubic diamond (cd) structure, to the higher pressure β-Sn structure, which occurs at 13 GPa on the hydrostat [1]. The crystal structures for these two phases are shown in figure 1. It should be noted that although we choose to refer to β-Sn in this paper, a similar analysis would apply to the closely related Imma phase, which is found to become stable between 15-32 GPa.

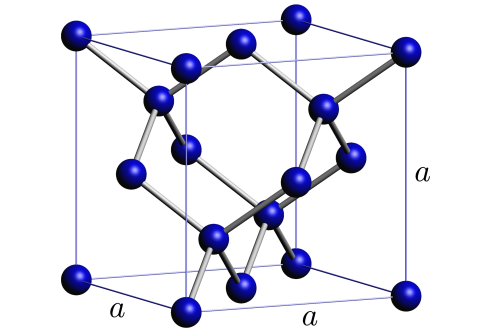

(a) Cubic diamond (cd)

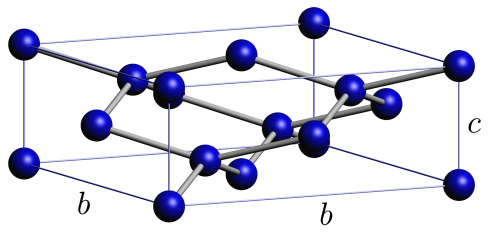

(b) Beta (β)

Figure 1: The two Si phases of interest. (a) The cubic diamond phase: a face-centered cubic lattice with a basis of $[(0,0,0),(\frac{1}{4},\frac{1}{4},\frac{1}{4})]$. (b) The β-Sn phase: a tetragonal lattice, with the same basis as cd. We use values of $a = 5.431$ Å, $b = 6.897$ Å and $c = 2.548$ Å, found by minimising the energy of the unit cell in MD, while holding the cell at zero external pressure.

Several features of this transition lead to complexity in its modelling. Firstly, silicon exhibits a large volume collapse of 21% between cd and β-Sn. Molecular dynamics simulations suggest that, for compression of single crystals along [001], this proceeds via a significant contraction along the compression direction, and an accompanying transverse expansion. Moreover, previous studies suggest a significant enthalpy barrier, and thus kinetic effects must be considered [12, 8].

In the following sections we will develop the theory of the Lagrangian elasticity (LE) code to allow for meaningful simulation of such a system.

2.2. Lagrangian Elasticity Code Formalism

The approach described here is based on the two step integration of the elasticity equations described by Horie [9, 10]. This method allows for solution of the 1d Lagrangian wave equations of Taylor [13] –

$$\rho_0 \left(\frac{\partial u}{\partial t}\right) + \left(\frac{\partial \sigma_n}{\partial z}\right) = 0, \tag{1}$$

$$\left(\frac{\partial u}{\partial z}\right) + e^{-\epsilon_n} \left(\frac{\partial \epsilon_n}{\partial t}\right) = 0, \tag{2}$$

where ρ_0 is the initial density of the material in a Lagrangian element, u is its position, σ_n the normal stress, and ϵ_n the normal true strain. Note the use of true, rather than engineering strain, leads to an additional factor of $e^{-\epsilon_n}$ not present in Taylor's description.

By utilising the equations of elasticity we can extend our model, tracking both longitudinal and transverse properties, while retaining a 1d integration scheme. We modify Taylor's treatment by considering a relation based on the full, strain dependent, compliance tensor, $\epsilon_i = S_{ij}(\bar{\epsilon})\sigma_j$. In order to allow for the strain dependence of the compliance tensor, we define the components in terms of small changes in stress and strain, which in the case of tetragonal symmetry gives –

$$\begin{pmatrix} \Delta\epsilon_t \\ \Delta\epsilon_t \\ \Delta\epsilon_n \\ 0 \\ 0 \\ 0 \end{pmatrix} = \begin{pmatrix} S_{11} & S_{12} & S_{13} & & & S_{16} \\ S_{12} & S_{11} & S_{13} & & & -S_{16} \\ S_{13} & S_{13} & S_{33} & & & \\ & & & S_{44} & & \\ & & & & S_{44} & \\ S_{16} & -S_{16} & & & & S_{66} \end{pmatrix} \begin{pmatrix} \Delta\sigma_t \\ \Delta\sigma_t \\ \Delta\sigma_n \\ 0 \\ 0 \\ 0 \end{pmatrix}. \tag{3}$$

where we have employed Voigt notation, and have defined $\epsilon_3 = \epsilon_n$ and $\epsilon_1 = \epsilon_2 = \epsilon_t$ (with similar definitions for the stress tensor), where subscripts n and t denote directions normal to and transverse to the compression direction respectively. We assume here that the stress and strain tensors are diagonalised, and that the two transverse stresses, and thus strains are equal. This leads to stress/strain relations of the form –

$$\Delta\epsilon_n = S_{33}\Delta\sigma_n + 2S_{13}\Delta\sigma_t, \tag{4a}$$

$$\Delta\epsilon_t = S_{13}\Delta\sigma_n + S_{1112}\Delta\sigma_t, \tag{4b}$$

where we have relabeled $(S_{11} + S_{12}) = S_{1112}$ to make clear that the relations require only three independent elastic

constants. These equations are analogous to eqn. 4 in ref. [10][1], where only two elastic constants are needed to describe a cubic system.

2.3. Phase transition

The formalism outlined above allows for integration of stress in a purely elastic solid. Previous work has used an additional model for plastic relaxation due to dislocation motion, however, in this work we will instead integrate a framework which allows us to describe relaxation via a solid-solid phase transition. In particular, we will allow for the existence of a mixed phase region, as required along a shock Hugoniot.

While the underlying principles of this model will work for an arbitrary number of phases it is sufficient here to consider only the two phases introduced above (Section 2.1). We calculate all strains as true strains, such that the extension ratio $\lambda = \frac{l}{l_0} = e^{-\epsilon}$.

The Lagrangian equations require the total longitudinal strain in the material. In the case of a mixed phase region we denote this as ϵ_n^m. This will be a combination of the extention ratios in the cd and β phases, weighted by the relative fraction of the two phases, such that –

$$e^{-\epsilon_n^m} \equiv \lambda_n^m = f\lambda_n^\beta + (1-f)\,\lambda_n^{\mathrm{cd}} + \chi\,(f)\,, \tag{5}$$

where the superscripts describe the phase, and the phase fraction, f where $0 < f < 1$, is the fraction of the material in the β-Sn phase. Additionally, we include a term, $\chi\,(f)$ which represents strain within boundaries between phases; material which is likely to be softer than can be described by a pure two phase elastic model. It is assumed that this boundary material fills a small volume fraction compared to the two bulk phases. This allows us to state that the fraction of material in the cubic diamond phase is $(1-f)$.

In addition to the total longitudinal strain, we can write the relationship between the transverse strains in the material –

$$\lambda_t^m = 1 = f\lambda_t^\beta + (1-f)\,\lambda_t^{\mathrm{cd}} + \chi\,(f)\,, \tag{6}$$

and we have included explicitly that $\epsilon_t^m = 0$, as required in the quasi-uniaxial experiments which this code was developed to simulate. Once again, we include the softer material at grain boundaries.

[1]It should be noted that the original paper [10] contains a typographical error in these equations, and that they should read, in the original nomenclature:

$$\sigma_n = \left(K + \frac{4\mu'}{3}\right)\epsilon_n^e + \left(2K - \frac{4\mu'}{3}\right)\epsilon_t^e,$$
$$\sigma_t = \left(K - \frac{2\mu'}{3}\right)\epsilon_n^e + \left(2K + \frac{2\mu'}{3}\right)\epsilon_t^e.$$

Taking derivates of equations 5 and 6 yields –

$$\lambda_n^m \Delta\epsilon_n^m = f\lambda_n^\beta \Delta\epsilon_n^\beta + (1-f)\lambda_n^{\mathrm{cd}}\Delta\epsilon_n^{\mathrm{cd}} + (\lambda_n^{\mathrm{cd}} - \lambda_n^\beta - \chi'\,(f))\Delta f, \tag{7a}$$

$$0 = f\lambda_t^\beta \Delta\epsilon_t^\beta + (1-f)\lambda_t^{\mathrm{cd}}\Delta\epsilon_t^{\mathrm{cd}} + (\lambda_t^{\mathrm{cd}} - \lambda_t^\beta - \chi'\,(f))\Delta f. \tag{7b}$$

The RHS of each of these equations is made up of three terms, each with clear meanings. The first term is the fraction of β phase with a given extension ratio, λ^β, (due to existing strain) multiplied by a change in strain $\Delta\epsilon^\beta$. The second term is the analogy for the cd phase. Finally the third term describes the volume collapse (or expansion) due to a small fraction, Δf, of the material changing from cd to β, with an associated dimension change $(\lambda^{\mathrm{cd}} - \lambda^\beta)$. It is this final term which accounts for the first order nature of the phase transition, and it will be seen to have important implications for the resultant wave profiles.

Combining these equations with the Lagrangian equations (eqns. 1 and 2), and our elasticity relations (eqn. 4) for each material, we arrive at the following relations between stress and strain in the material –

$$\Delta\sigma_n = \frac{\lambda_n^m \Delta\epsilon_n^m - (\lambda_n^{\mathrm{cd}} - \lambda_n^\beta - \chi'\,(f))\Delta f - A}{B} \tag{8}$$

$$\Delta\sigma_t = -\frac{\Lambda_{t,13}\Delta\sigma_n + (\lambda_t^{\mathrm{cd}} - \lambda_t^\beta - \chi'\,(f))\Delta f}{\Lambda_{t,1112}} \tag{9}$$

where

$$A = -\frac{2\Lambda_{n,13}(\lambda_t^{\mathrm{cd}} - \lambda_t^\beta - \chi'\,(f))\Delta f}{\Lambda_{t,1112}}, \tag{10}$$

$$B = \Lambda_{n,33} - \frac{2\Lambda_{t,13}\Lambda_{n,13}}{\Lambda_{t,1112}}, \tag{11}$$

$$\Lambda_{d,ij} = f\lambda_d^\beta S_{ij}^\beta + (1-f)\lambda_d^{\mathrm{cd}} S_{ij}^{\mathrm{cd}} \tag{12}$$

with $d = n, t$ and $ij = 13, 33, 1112$.

Note that we only calculate a single stress tensor for the sample. We therefore assume that the two phases are in the Reuss limit [14], that is the limit of iso-stress between phases. While this may be a simplification, molecular dynamics simulations, described below, show no significant departure from this limit, and its use is justified by the quality of fit it affords between the two simulation methods.

Given the imposed boundary condition $\sigma_n(z = 0, t)$, an integration step proceeds as follows for each cell: if there is any shear stress in the cell, the phase fraction is adjusted to relieve this stress using eqn. 13; the change in longitudinal strain is then calculated following the arguments laid out by Horie [9]; the changes in normal and transverse stress are calculated using eqns. 4 and 7; finally the changes to the individual phase's strains are adjusted using eqn. 4. An algorithmic representation of one simulation timestep is shown in Appendix Appendix A.

2.4. Calculating the elastic constants

The code described above requires as an input the strain dependent elastic constants for each phase. Since we will ultimately aim to benchmark the LE code against classical molecular dynamics (MD) we will take our elastic constants from the empirical potential used for these MD simulations.

The elastic constants, S_{ij}, are calculated using the LAMMPS code [15], the same code that we use to run MD shock simulations. The interatomic interactions were modelled using a Tersoff-like potential [16], as parameterised by Erhart and Albe [17].

By initialising a unit cell of silicon atoms in a strained cubic diamond crystal structure, then applying infinitesimal strains to the unit cell and measuring the change in the stress tensor, the relevant S_{ij} can be calculated for any position in the (ϵ_n, ϵ_t)-space.

The elastic constants were calculated at 0 K. While methods do exist to reliably calculate elastic constants at finite temperature, such as those of Zhen and Chu [18], as we are concerned with low (300 K) temperatures, a simpler approach is sufficient. Small, linear temperature dependencies were imposed on the elastic constants to match the elastic wave speed from MD. The values that result in good agreement with the elastic wave speed lie between those calculated separately by Toupance [19] and Schall *et al.* [20], and are on the order of 10 MPaK^{-1}.

2.5. Fitting parameters

The model above must be supplemented with empirical models which govern rate of phase change, and softening of boundaries. It is these models which provide free fitting parameters to match the code to MD or experiment.

Given the significant enthalpy barrier of the cd→ β-Sn transition, we must take into account kinetics. In order to achieve this we allow for a 'lag' between the material reaching the threshold pressure for phase transition, and the onset of growth of the new phase. Once a cell's pressure has been above the transition pressure, σ^*, for at least this lag time, τ, an increasing phase fraction is driven by the non-zero shear stress, $(\sigma_n - \sigma_t)$, according to –

$$\Delta f = \begin{cases} \kappa \Delta t (\sigma_n - \sigma_t), & \text{if } \sigma_n > \sigma^* \\ 0, & \text{otherwise} \end{cases} \qquad (13)$$

where κ is a constant which governs the rate of growth of the phase, and Δt is time-resolution of the simulation.

The phase boundary softening term takes a simple functional form

$$\chi(f) = \mu \sin^2(\pi f) \qquad (14)$$

This allows for description of grain boundary softening with single free parameter, μ, whilst ensuring that the effect is only significant in mixed phase regions.

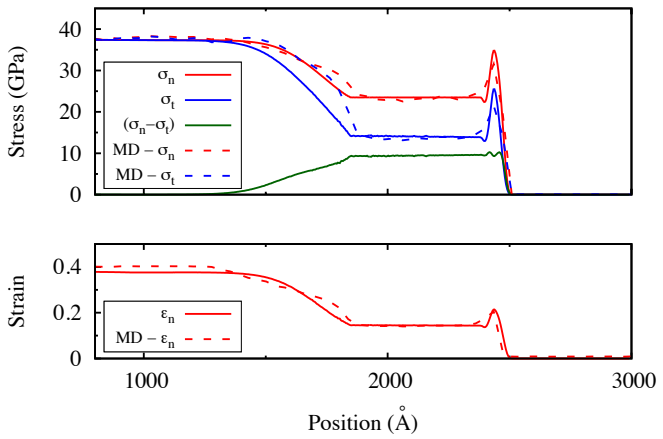

Figure 2: Output from the LE code (solid lines) compared with output from the MD simulations (dashed lines) at peak longitudinal stress of 37.5 GPa.

This leaves four fitting parameters, κ, σ^*, τ and μ, to describe phase change kinetics and dynamics, and elasticity at phase boundaries. The effect of each parameter on wave profiles is distinct, and as such, solutions unique.

It should be noted that it would be possible in principle to use more complex models (such as a stochastic or stress dependent models for lag time).

3. Comparison of Lagrangian elastic code with MD simulations

MD simulations were conducted using the LAMMPS code with a sample size was 30x30x400 unit cells (2,881,800 atoms). The sample was thermalised at 300K, before a fixed pressure (as opposed to the frequently used fixed velocity) piston was applied at position $z = 0$, launching a shock along the [001] crystallographic direction. As has been observed in previous work [21], these simulations display a phase transition to Imma at 31 GPa, with a significant mixed phase region visible. As such, they provide an ideal testbed for the LE formalism.

The corresponding LE code features 1000 Lagrangian cells, and runs with temporal and spatial resolutions of 0.01 ps and 0.5 nm respectively. It is important to note that we have determined that varying the temporal and spatial resolutions of the simulation has no effect on the phase change. The simulations run a factor of 10^4 times faster than the corresponding MD.

We show a comparison of the two simulation methods in figure 2, for a piston held at a fixed pressure of 37.5 GPa. A good agreement between the two stress profiles is seen, as well as the longitudinal strain profiles. The slight discrepancy between the final strains is due to melting of the material in MD, which is not accounted for by the two-phase model in the LE code. In figure 3, we show a comparison between the two codes for multiple timesteps throughout the simulations, which again show good agreement. We

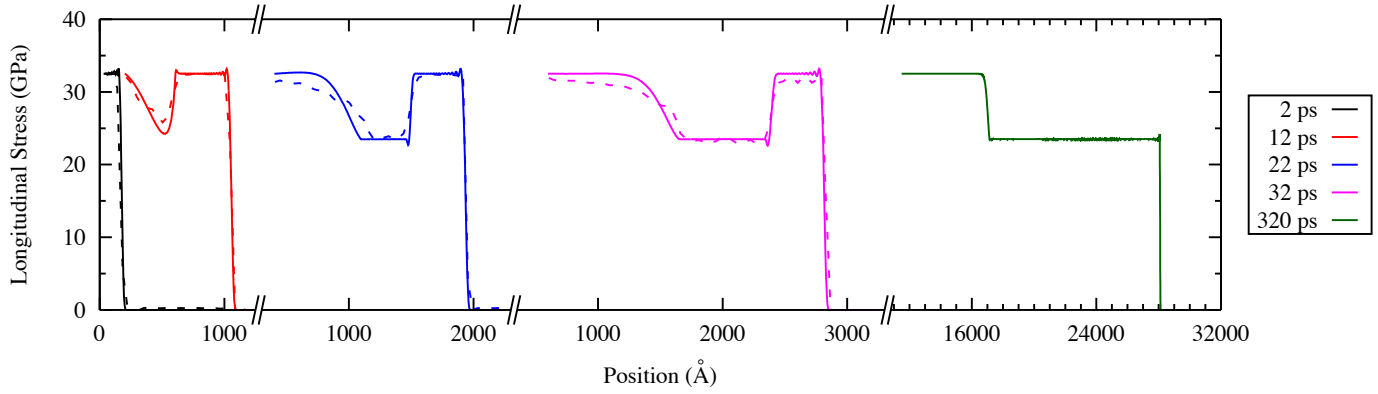

Figure 3: Longitudinal stress profiles from the LE code (solid lines) compared with output from the MD simulations (dashed lines) at peak longitudinal stress of 32 GPa. Also shown is a late-time profile to show the erosion of the preceding high-strain elastic plateau, where we have rescaled the abscissa to include the full elastic plateau. MD simulations were not possible at this final scale.

can see that for a lower pressure piston, here 32.5 GPa, the delay before the onset of the phase change is longer than for the higher pressure piston shown in figure 2, resulting in a longer high-strain elastic plateau (HSE). Also shown is the wave profile that develops at longer time- and length-scales, where the HSE is fully eroded by the fast-moving partial release wave. It is this complete erosion of the HSE, on the length-scales of gas gun experiments, that accounts for the absence of the "anomalous elastic response" in such experiments. The values of the fitting parameters used in these simulations were: $\sigma^* = 23.5$ GPa, $\kappa = 8\times10^{-3}$ ps^{-1} GPa^{-1}, $\mu = -0.042$, and $\tau = 0.4$ ps (37.5 GPa piston) and 6.0 ps (32.5 GPa piston). We note that the small value of μ implies that the boundaries between phases account for only a small fraction of the total volume, as previously suggested.

We highlight the ability for the LE code to predict the longitudinal and transverse strain in each of the phases. These are measured relative to the dimensions of ambient cubic diamond, and shown in figure 4. We can see that the onset of the phase transition allows the initially uniaxially strained cd phase to return to the hydrostat. It is this calculation of the strains that allows x-ray diffraction from the sample to be simulated, for further details see fig. 3 in ref. [8].

Also in figure 4, we compare the volume fraction, f^V, of the β-Sn fraction in the LE simulations with that calculated from the corresponding MD simulation. The volume fraction is related to the phase fraction in the code, f, as detailed in appendix Appendix B. The discrepancy in volume fraction between the two simulation methods, seen immediately ahead of the piston in figure 4, is again due to the onset of melting in the MD simulations, a process which is not accounted for in the two-phase model introduced here.

It should be noted that in the published MD simulations [21], small rotations of each phase, about an axis perpendicular to the drive direction, are observed in the mixed-phase region, which further allow the region to accommodate the high shear stress. These rotations can not be taken into account in this 1D formulation.

Additionally, we note that in the same work, while a change of basis is observed which is consistent with a move towards *Imma*, the cell remains largely tetragonal, with the two transverse cell dimensions measured to be the same. We must be careful to separate the change in position of the basis atoms from β-Sn to *Imma*, which is seen in the MD, with the opportunity for *Imma* to move away from tetragonal symmetry towards orthorhombic, which is not seen. In any case, as the pressures in the MD simulations far exceed the experimental conditions at which either structure is observed, these studies should not be seen as an indication of phase stability at these pressures.

4. Conclusions

In this paper we present a full description of a new Lagrangian elastic (LE) code which aims to bridge the gap between traditional hydrocodes and computationally expensive molecular dynamics (MD) simulations, and focus on its ability to simulate solid-solid phase changes, and the resulting mixed-phase regions.

We combine the 1D Lagrangian wave equations with Hooke's Law and an equation that governs the phase change, to form a closed set of equations that can be integrated numerically to calculate the stresses and strains in uniaxially compressed solid targets. We compare the output of this LE code with that of MD simulations run using the LAMMPS code, and find good agreement.

Finally, we illustrate the LE code's intrinsic ability to calculate and store the strains in each phase following the phase change, a feature that traditional hydrocodes, using multi-phase equations of state, lack. As one of the major diagnostics in shock wave experiments is x-ray diffraction,

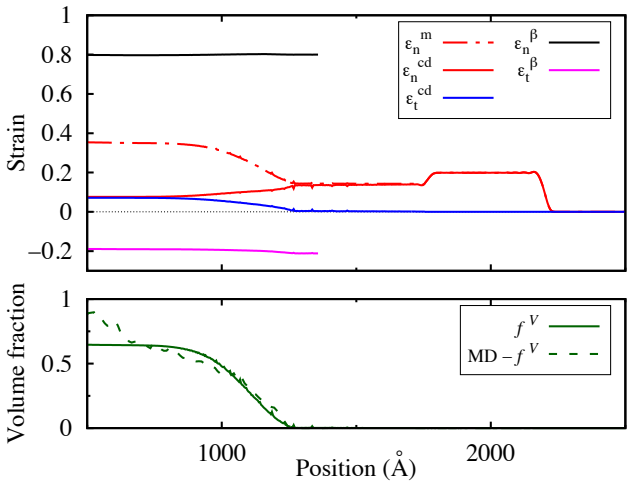

Figure 4: The normal and transverse strains in each of the phases, along with the total phase fraction, for the simulation shown in FIG. 3. We can see that the onset of the phase change allows the initially uniaxially strained cd phase to return to the hydrostat, with $\epsilon_n^{\mathrm{cd}} = \epsilon_t^{\mathrm{cd}}$. The volume fraction from the LE code is compared with that measured from MD in the lower plot.

and the diffraction pattern from a sample is directly related to the strains contained within, the ability to calculate the individual phases' strains is crucial to enable simulated diffraction patterns to be created, which can then be compared with experimental diffraction data.

The model is applicable to any polymorphic phase transition that conserves the number of unit cells transverse to the shock. Also, the formalism could, in principle, accommodate multiple phase changes and mixed phase regions consisting of more than two phases.

Acknowledgements

PGS would like to thank AWE for financial support. JSW is grateful for support from EPSRC under grant EP/J017256/1

References

[1] A Mujica. High-pressure phases of group-IV , III – V , and II – VI compounds. *Reviews of Modern Physics*, 75(July), 2003.

[2] GJ Auckland. High-pressure phases of group IV and III-V semiconductors. *Reports on Progress in Physics*, 64(4):483–516, 2001. ISSN 0034-4885. doi:10.1088/0034-4885/64/4/202. URL `http://apps.webofknowledge.com/full{_}record.do?product=UA{&}search{_}mode=CitingArticles{&}qid=25{&}SID=W1iC7owbanWJugwxXoq{&}page=2{&}doc=19$\delimiter"026E30F$nhttp://iopscience.iop.org/0034-4885/64/4/202/pdf/0034-4885{_}64{_}4{_}202.pdf`.

[3] M. N. Pavlovskii. Formation of metallic modification of Germanium and Silicon under shock loading, 1967.

[4] W. H. Gust. Axial Yield Strengths and Two Successive Phase Transition Stresses for Crystalline Silicon. *Journal of Applied Physics*, 42(5):1897, 1971. ISSN 00218979. doi:10.1063/1.1660465. URL `http://scitation.aip.org/content/aip/journal/jap/42/5/10.1063/1.1660465`.

[5] Stefan J. Turneaure and Y. M. Gupta. Inelastic deformation and phase transformation of shock compressed silicon single crystals. *Applied Physics Letters*, 91(20):201913, 2007. ISSN 00036951. doi:10.1063/1.2814067. URL `http://scitation.aip.org/content/aip/journal/apl/91/20/10.1063/1.2814067`.

[6] Stefan J. Turneaure and Y. M. Gupta. Real-time x-ray diffraction at the impact surface of shocked crystals. *Journal of Applied Physics*, 111(2):026101, 2012. ISSN 00218979. doi:10.1063/1.3674276. URL `http://scitation.aip.org/content/aip/journal/jap/111/2/10.1063/1.3674276`.

[7] A. Loveridge-Smith, A. Allen, J. Belak, T. Boehly, A. Hauer, B. Holian, D. Kalantar, G. Kyrala, R. Lee, P. Lomdahl, M. Meyers, D. Paisley, S. Pollaine, B. Remington, D. Swift, S. Weber, and J. Wark. Anomalous Elastic Response of Silicon to Uniaxial Shock Compression on Nanosecond Time Scales. *Physical Review Letters*, 86(11):2349–2352, Mar 2001. ISSN 0031-9007. doi:10.1103/PhysRevLett.86.2349. URL `http://link.aps.org/doi/10.1103/PhysRevLett.86.2349`.

[8] A. Higginbotham, P. G. Stubley, A. J. Comley, J. H. Eggert, J. M. Foster, D. H. Kalantar, D. McGonegle, S. Patel, L. J. Peacock, S. D. Rothman, R. F. Smith, M. J. Suggit, and J. S. Wark. Inelastic response of silicon to shock compression. *Scientific Reports*, 6(April):24211, 2016. ISSN 2045-2322. doi:10.1038/srep24211. URL `http://www.nature.com/articles/srep24211`.

[9] Y. Horie. Numerical Integration of Plane Elastic-Relaxing Plastic Shock Waves by a Two-Step Method. *Journal of Applied Physics*, 40(13):5368, 1969. ISSN 00218979. doi:10.1063/1.1657396. URL `http://link.aip.org/link/?JAP/40/5368/1&Agg=doi`.

[10] Justin S Wark, Andrew Higginbotham, Despina Milathianaki, and Arianna Gleason. Combined hydrodynamic and diffraction simulations of femtosecond x-ray scattering from laser-shocked crystals. *Journal of Physics: Conference Series*, 500 (15):152016, 2014. URL `http://stacks.iop.org/1742-6596/500/i=15/a=152016`.

[11] D Milathianaki, S Boutet, G J Williams, A Higginbotham, D Ratner, A E Gleason, M Messerschmidt, M M Seibert, D C Swift, P Hering, J Robinson, W E White, and J S Wark. Femtosecond visualization of lattice dynamics in shock-compressed matter. *Science (New York, N.Y.)*, 342(6155):220–3, October 2013. ISSN 1095-9203. doi:10.1126/science.1239566. URL `http://www.ncbi.nlm.nih.gov/pubmed/24115435`.

[12] K. Gaál-Nagy, A. Bauer, P. Pavone, and D. Strauch. Ab initio study of the enthalpy barriers of the high-pressure phase transition from the cubic-diamond to the beta-tin structure of silicon and germanium. *Computational Materials Science*, 30(1-2 SPEC ISS.):1–7, 2004. ISSN 09270256. doi:10.1016/j.commatsci.2004.01.002.

[13] John W. Taylor. Dislocation Dynamics and Dynamic Yielding. *Journal of Applied Physics*, 36(10):3146, 1965. ISSN 00218979. doi:10.1063/1.1702940. URL `http://link.aip.org/link/JAPIAU/v36/i10/p3146/s1&Agg=doi`.

[14] A Reuss. Berechnung der fließgrenze von mischkristallen auf grund der plastizitätsbedingung für einkristalle. *ZAMM-Journal of Applied Mathematics and Mechanics/Zeitschrift für Angewandte Mathematik und Mechanik*, 9(1):49–58, 1929.

[15] Steve Plimpton. Fast Parallel Algorithms for Short – Range Molecular Dynamics. *Journal of Computational Physics*, 117(June 1994):1–19, 1995. ISSN 00219991. doi:10.1006/jcph.1995.1039.

[16] J. Tersoff. New empirical approach for the structure and energy of covalent systems. *Physical Review B*, 37(12):6991–7000, 1988. ISSN 01631829. doi:10.1103/PhysRevB.37.6991. URL `http://journals.aps.org/prb/pdf/10.1103/PhysRevB.37.6991`.

[17] P Erhart and K Albe. Analytical potential for atomistic simulations of silicon, carbon, and silicon carbide. *Physical Review B*, 71(3):35211, 2005. ISSN 1098-0121. doi:10.1103/PhysRevB.71.035211. URL `http:`

//scitation.aip.org/getabs/servlet/GetabsServlet?prog=normal{&}id=PRBMDO000071000003035211000001{&}idtype=cvips{&}gifs=yes$\delimiter"026E30F$npapers://e21c739b-a592-49dd-9869-dfc7822cc78f/Paper/p563.

[18] Yubao Zhen and Chengbiao Chu. A deformation–fluctuation hybrid method for fast evaluation of elastic constants with many-body potentials. *Computer Physics Communications*, 183(2):261–265, 2012. ISSN 00104655. doi:10.1016/j.cpc.2011.09.006. URL http://linkinghub.elsevier.com/retrieve/pii/S0010465511003249.

[19] N. Toupance. Temperature Dependence of the Elastic Constants. *phys. stat. sol*, 1987. doi:10.1103/PhysRevB.2.3952. URL http://link.aps.org/doi/10.1103/PhysRevB.2.3952.

[20] J. David Schall, Guangtu Gao, and Judith a. Harrison. Elastic constants of silicon materials calculated as a function of temperature using a parametrization of the second-generation reactive empirical bond-order potential. *Physical Review B - Condensed Matter and Materials Physics*, 77:1–19, 2008. ISSN 10980121. doi:10.1103/PhysRevB.77.115209.

[21] Gabriele Mogni, Andrew Higginbotham, Katalin Gaál-Nagy, Nigel Park, and Justin S. Wark. Molecular dynamics simulations of shock-compressed single-crystal silicon. *Physical Review B*, 89(6):064104, feb 2014. ISSN 1098-0121. doi:10.1103/PhysRevB.89.064104. URL http://link.aps.org/doi/10.1103/PhysRevB.89.064104.

Appendix A. The integration routine - Algorithmic form

Given the imposed boundary condition $\sigma_n(z=0,t)$, an integration step at timestep $t=l$ proceeds as follows, assuming a total number of spatial cells N –

for $j \leftarrow 1$ to $N-1$:

$$\Delta f \leftarrow \kappa \Delta t(\sigma_n - \sigma_t),$$

$$\Delta\epsilon^m_{n,j}(t=l) \leftarrow \frac{R^2}{\rho_0}\sum_{k=0}^{l}(\sigma^k_{n,j+1} - 2\sigma^k_{n,j} + \sigma^k_{n,j-1}),$$

$$\Delta\sigma_n \leftarrow \frac{\lambda^m_n \Delta\epsilon^m_n - (\lambda^{\mathrm{cd}}_n - \lambda^\beta_n - \chi'(f))\Delta f - A}{B},$$

$$\Delta\sigma_t \leftarrow -\frac{\Lambda_{t,13}\Delta\sigma_n + (\lambda^{\mathrm{cd}}_t - \lambda^\beta_t - \chi'(f))\Delta f}{\Lambda_{t,1112}},$$

$$\Delta\epsilon^{\mathrm{cd},\beta}_n \leftarrow S^{\mathrm{cd},\beta}_{33}\Delta\sigma_n + 2S^{\mathrm{cd},\beta}_{13}\Delta\sigma_t,$$

$$\Delta\epsilon^{\mathrm{cd},\beta}_t \leftarrow S^{\mathrm{cd},\beta}_{13}\Delta\sigma_n + S^{\mathrm{cd},\beta}_{1112}\Delta\sigma_t,$$

where cell number j is an implicit subscript, and timestep l an implicit superscript, of all variables except where shown explicitly in the second equation, which follows from the arguments set out by Horie [9]. $R = \Delta t/\Delta x$ is the ratio of the temporal and spatial resolutions of the simulation. All parameters are then incremented, *e.g.* $\sigma_n \leftarrow \sigma_n + \Delta\sigma_n$, and the routine repeats for timestep $t = l+1$.

Appendix B. Relating the volume fraction and the phase fraction

As the phase fraction in the LE code is a description of the fraction of phase in any one dimension, it must be converted to a volume fraction for direct comparison with MD. First we note that the average unit cell volume, V, is related to the unit cell volumes of the two phases, V^{cd} and V^β, and the number fraction (the fraction of unit cells in the sample which are β-Sn phase), f^N, by the following expression –

$$V = f^N V^\beta + (1-f^N)V^{\mathrm{cd}} \tag{B.1}$$

$$\Rightarrow f^N = \frac{V - V^{\mathrm{cd}}}{V^\beta - V^{\mathrm{cd}}}. \tag{B.2}$$

As noted in the work of Mogni *et al.* [21], the volume fraction, f^V, is related to the number fraction, f^N, by –

$$f^V = \frac{f^N V^\beta}{f^N V^\beta + (1-f^N)V^{\mathrm{cd}}}. \tag{B.3}$$

This volume fraction is compared with that calculated from MD in figure 4.